International Journal of
High-Rise Buildings
www.ctbuh-korea.org/ijhrb/index.php

International Journal of High-Rise Buildings
December 2022, Vol 11, No 4, 301-314
https://doi.org/10.21022/IJHRB.2022.11.4.301

Verification of Speed-up Mechanism of Pedestrian-level Winds Around Square Buildings by CFD

Hideyuki Tanaka[1], Qiang Lin[2†], Yasuhiko Azegami[3], and Yukio Tamura[4]

[1]*Takenaka Research & Development Institute, Takenaka Corporation*
[2]*School of Civil Engineering, Chongqing University*
[3]*Takenaka Research & Development Institute, Takenaka Corporation*
[4]*School of Civil Engineering, Chongqing University*

Abstract Various studies have been conducted on pedestrian-level wind environments around buildings. With regard to the speed-up mechanism of pedestrian-level winds, there are references to downwash effect due to the vertical pressure gradient of boundary layer flow and venturi effect due to flow blocking by the building. Two factors contribute to increase or decrease of downwash effect: change in two-dimensional / three-dimensional air flow pattern (Type 1) and change in downwash wind speed due to building size that does not accompany change in airflow pattern (Type 2). Previous studies have shown that downwash effect has a greater influence in increasing or decreasing the area of strong wind than venturi effect. However, these considerations are derived from the horizontal mean wind speed distribution at pedestrian level and are not the result of three-dimensional flow field around the building. Therefore, in this study, Computational Fluid Dynamics using Large Eddy Simulation were performed to verify the downwash phenomena that contributes to increase in wind speed at pedestrian level.

Keywords **Pedestrian wind environment, Downwash effect, Venturi effect, speed-up ratio, speed-up area, LES**

[†]Corresponding author:
Qiang Lin
linqiang@cqu.edu.cn

1. Introduction

A large number of high-rise and super high-rise buildings have been constructed in cities due to the increasing demand for housing and commercial space. However, high-rise buildings in cities tend to introduce high-speed wind from high elevations to ground level, creating uncomfortable and even unsafe wind conditions for pedestrians (Wise., 1970; Lawson., 1978). High wind speed at pedestrian-level is one of the problems that is considered most important for improving pedestrian wind environments around tall buildings.

Pedestrian wind environments have caused great concern since the 1960s. Extensive researches have been conducted to investigate the characteristics of pedestrian-level wind around high-rise buildings by full-scale measurements (Isyumov & Davenport., 1975; Murakami et al., 1979), wind tunnel tests (Kamei & Maruta., 1979; Tsang et al., 2012; Tamura et al., 2019), and computational fluid dynamics (CFD) (Yoshie et al., 2007; Blocken., 2014; Cui et al., 2019), and several assessment criteria for pedestrian wind comfort, based on threshold mean or gust wind speeds and the probabilities of exceedance, have also been proposed (e.g. Isyumov & Davenport., 1975; Melbourne., 1978; Lawson., 1978; Murakami et al., 1986; NEN 8100., 2006; Du et al., 2017). Some of these studies have mentioned the physical mechanisms of speed-up phenomena at pedestrian level, which are essential to understand in order to take measures to mitigate pedestrian discomfort. These mechanisms include downwash effect (or down flow) due to the pressure gradient in the boundary layer flow and venturi effect due to the narrowing flow section created by the presence of buildings (e.g., Wise, 1970., Beranek., 1984; Cook., 1985; Blocken et al., 2008). In this paper, "Venturi effect" means the speed-up phenomenon due to the existence of a building that blocks the approaching flow, forcing it through a narrower path than the upstream region. This phenomenon is most significant in shear layers separated from the leading edges of building sections. Therefore, it may also be called "Separated Shear Layer Effect". However, the separated shear layer is not so strong in some cases, so this effect is simply named "Venturi

Effect" following Tamura et al. (2019). More recently, Tamura et al. (2019) identified two types of variations of downwash effects with building configurations and found that downwash effect is more significant than venturi effect for isolated high-rise buildings. However, these findings were derived based only on measured mean pedestrian-level wind speeds around high-rise buildings and they have not confirmed the two types of variations of downwash effect by examining flow patterns. It is known that flow fields even around isolated buildings are complicated.

Studies on flow fields around square-section or other types of bluff bodies have mainly focused on wake flows under uniform approaching flows (Wang et al., 2006; Bourgeois et al., 2011; Summer et al., 2017) and turbulent boundary layer flows (Kawai et al., 2012), since their main aims were to investigate the relationship between wake flow structures and aerodynamic characteristics of buildings. Flow-field studies on pedestrian wind environments have mainly focused on one or several specified planes of high-rise buildings (Kim et al., 2019; Cui et al., 2019) or low-rise buildings (Liu et al., 2020), not on overall flow structures around buildings. However, high pedestrian-level winds are mainly caused by downwash flow starting near the front stagnation point on the windward surface and flowing toward the ground and around both sides. The flows around the sides are separated from the windward corners of the building and form a wake region. Therefore, it is necessary to investigate the overall flow fields around high-rise buildings to clarify the downwash flow structure that is blocked by buildings and accelerates pedestrian-level winds, and more studies on flow fields around high-rise buildings in boundary layer wind conditions are needed.

In addition, not only mean flows around buildings, but also instantaneous flow patterns are important to examine downwash effect causing strong wind conditions near the ground, and fluctuating pedestrian-level winds are also vital for evaluating wind effects on pedestrians. Therefore, it was necessary to verify the previous findings on variations of downwash effect by using suitable methods that could predict transient and complex flows around buildings. With the development of computer techniques and the support of several best practice guidelines (e.g. NEN8100., 2006; Tominaga et al., 2008), the CFD method has gained increasing acceptance for pedestrian level wind environmental studies. At present, the Reynolds-averaged Navier-Stokes (RANS) has been the most commonly used approach in CFD for pedestrian level wind environmental studies due to its reasonable computational cost and accuracy in predicting flows in high-speed regions, but it cannot model the inherently transient features of the flow field. This will cause inaccurate results, especially for complex and unsteady flows around buildings (Blocken., 2018). Large eddy simulation (LES), in which the scales of motion larger than grid size are directly resolved and the smaller scales of motion are modeled by adopting a sub-grid scale (SGS) model, can overcome the shortcomings of RANS to some extent and can be used to model turbulent flows around buildings. Many researchers have investigated air flows around a bluff body by using LES (Tominaga et al., 2010; Hu et al., 2015; Cao et al., 2016; Liu et al., 2016; Hooff et al., 2017). However, there have been insufficient studies using the LES approach to comparatively clarify the overall flow structures around high-rise buildings with special focus on pedestrian-level wind.

Therefore, a numerical study based on LES in CFD was conducted for square-section high-rise buildings with aspect ratios of 1-16 by directly examining the flow patterns around buildings to validate the Type 1 variation of downwash effect reported by Tamura et al. (2019) in this paper. Prior to this, the reliability of CFD results was confirmed by comparing CFD results with wind tunnel results of Tamura et al. (2019).

2. Overview of Numerical Simulations

2.1. Target Buildings

The square-section building models used in this study have the same height $H_0 = 160$ m but different widths varying from $B = 10$ m to $B = 160$ m, giving width ratios $B/H_0 = 0.0625$~1 (or aspect ratios $H_0/B = 1$~16), as shown in Table 1. Numerical calculations were conducted for all these building models in boundary layer flow (BLF). In addition, corresponding calculations for building models with $B/H_0 = 0.25$ ($H_0/B = 4$) in uniform turbulent flow (UTF) were also performed as a comparison with the flow characteristics around the building model in BLF. Only one wind direction was examined: that facing the building. The coordinate system was set at intersection point ($x/B_0 = 0$, $y/B_0 = 0$, $z/H_0 = 0$) for the ground surface, windward surface and vertical center surface of the building models, defined as x (streamwise direction), y (across-wind direction), and z (vertical direction). Here, B_0 is the reference building width used for standardization, defined as building width of B_0=20 m with width ratio $B/H_0 = 0.125$ ($H_0/B = 8$).

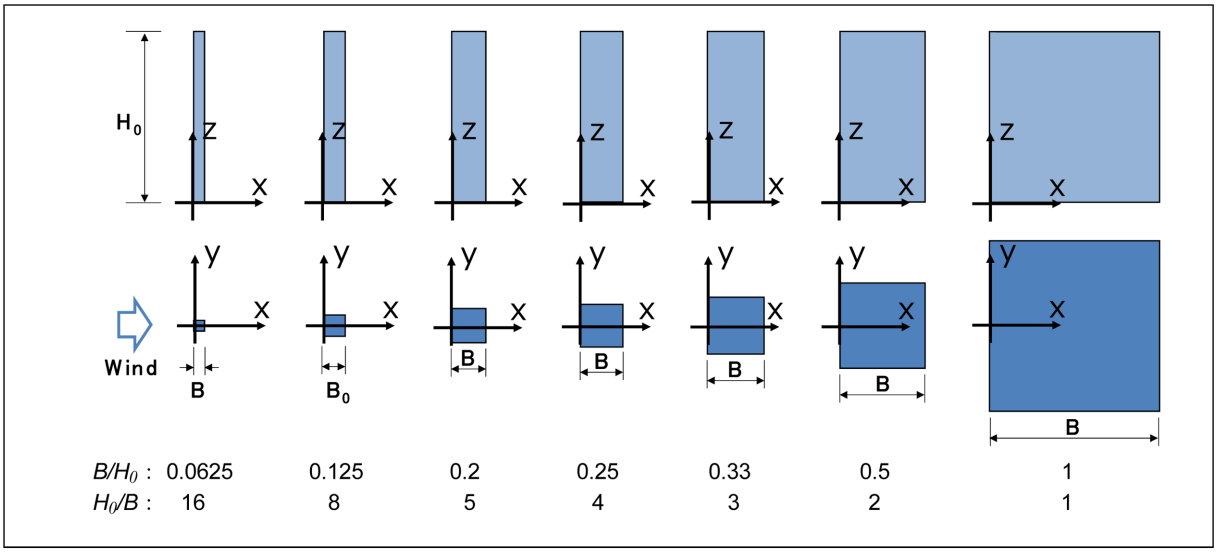
2.2. Simulation Conditions

The numerical setting details are shown in Table 2. In this study, the computational fluid dynamics (CFD) code (Tanaka et al., 2013, 2014) is used. A brief introduction to the numerical simulation method is given in Table 2. The Coherent Structured Smagorinsky model (Kobayashi, 2005) is used for the SGS model of LES.

The four different simulation fields examined in this study are shown in Fig. 1, and their sizes and boundary conditions are shown in Table 3. Sufficient distances between building surfaces and boundaries of the computational domain are secured by referring to the Guidebook for CFD (Architectural Institute of Japan, 2016). The approaching flow conditions at the inflow boundary ($x/$

Table 1. Target buildings

B/H_0	0.0625	0.125	0.2	0.25	0.33	0.5	1
H_0/B	16	8	5	4	3	2	1
B(m)	10	20 (= B_0)	32	40	53.3	80	160
H_0(m)	160	160	160	160	160	160	160
Flow	BLF	BLF	BLF	BLF UTF	BLF	BLF	BLF



$B_0 = -30$) are the same as those in the wind tunnel experiments by Tamura et al. (2019), that is, boundary layer flow (BLF) simulating an urban area and uniform turbulent flow (UTF). Fig. 2 shows the vertical distributions of mean wind speed U/U_H and the turbulence intensity I_U in the streamwise direction, and the values of mean wind speed U_H and turbulence intensity I_{UH} at building height H in BLF and UTF are shown in Table 3. The power-law exponent of the mean wind speed profile of BLF was 0.27, representing the urban terrain condition. The inflow fluctuations used in the present study are separately calculated and generated by a precursor LES reproducing the inside of a wind tunnel facility (e.g., Tanaka et al., 2013).

For the BLF cases, the resistance due to the roughness blocks shown in Fig. 1(a) is modeled on the upwind side floor of the building models (Maruyama, 2004), so that the turbulence characteristics given as inflow boundary conditions can be maintained. On the other hand, for the UTF cases, no resistance such as roughness blocks are provided on the upwind side floor, as shown in Fig. 1(b), in order to maintain flow uniformity.

Fig. 3 shows the vertical distribution of approaching flow characteristics at the origin ($x/B_0 = 0, y/B_0 = 0$) simulated without the target buildings, as shown in Figs. 1(c) and 1(d). Although the effect of the fetch surface can be seen in the distribution of U/U_H and I_U near the ground for both BLF and UTF, the turbulence characteristics of the inflow boundary conditions in Fig. 2 are sufficiently maintained, and the mean wind speed $U_{z=2\,\mathrm{m}}$ in the streamwise direction at pedestrian level z/H=0.0125

Table 2. Simulation settings

Algorism	Finite Difference Method (FDM)
Code	Kazamidori® (in-house code)
Turbulence model	Large Eddy Simulation (LES)
SGS model	Coherent structured Smagorinsky (Kobayashi, 2005)
Spatial difference scheme	30% of 3rd order upwind difference and 4th order centered difference scheme
Time scheme	3rd order Adams-Bashforth method and Clank-Nicolson method
Poisson solver	Residual cutting method
Grid system	Non-uniform staggered grid system (Kajishima, 1999)

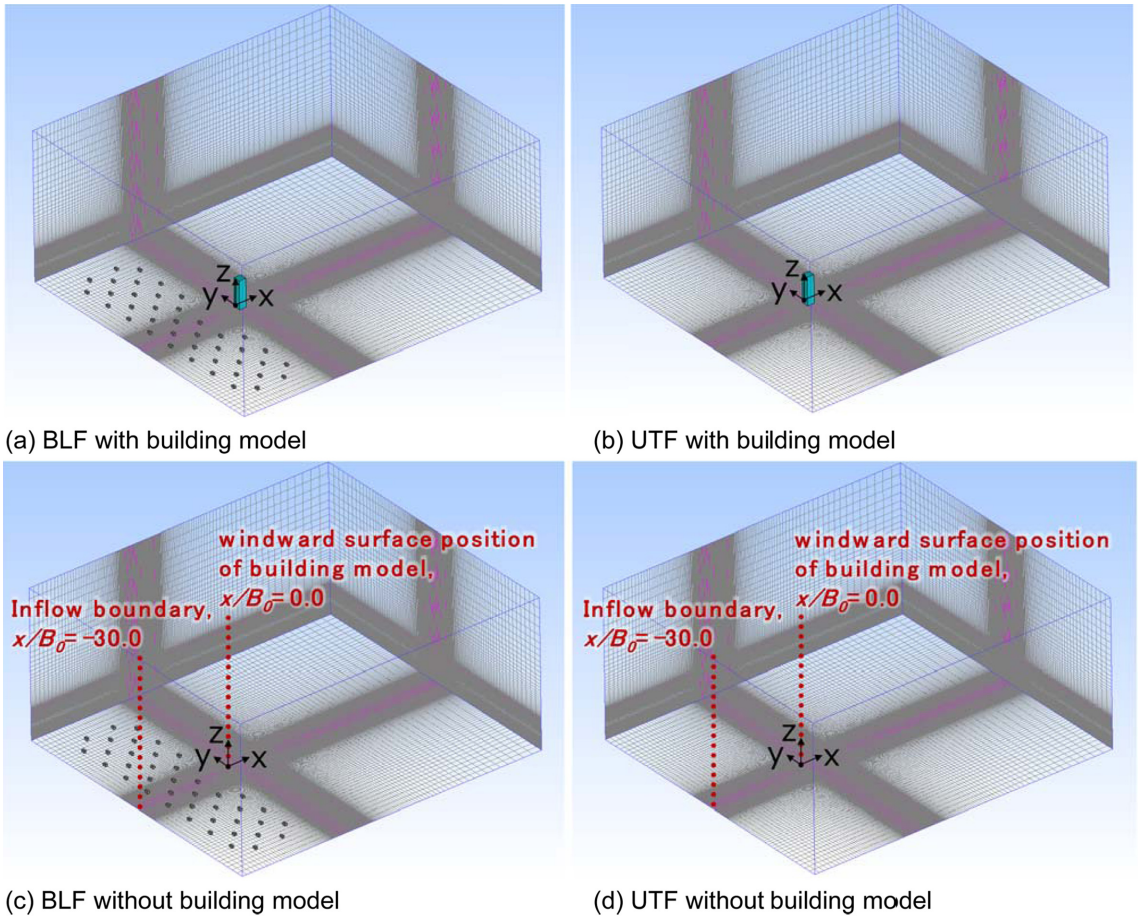


Figure 1. Computational domain.

Table 3. Simulation conditions

Calculation domain	$90B_0$ (x) × $80B_0$ (y) × $5.25H_0$ (z)
Grid number	About 1.4×10^7
Minimum grid size	$0.02B_0$
Calculation time	About 10min in full-scale × 6waves
Time interval	4×10^{-5}s
Inflow boundary	Artificially generated inflow BLF : U_H = 10 m/s, $U(z) = U_H(z/H)^{0.27}$, I_{UH} = 15% UTF : U_H = 10 m/s, I_{UH} = 11%
Downstream boundary	Convective boundary conditions
Lateral and upper surface boundaries	Zero gradient condition
Ground and building surface boundaries	Wall function (two-layer model)

(z = 2 m) is used to normalize the wind speeds. Note that the mean wind speeds $U_{z=2m}$ at the pedestrian-level of BLF and UTF were 3.8 m/s and 7.4 m/s, respectively.

3. Simulation Results and Discussions

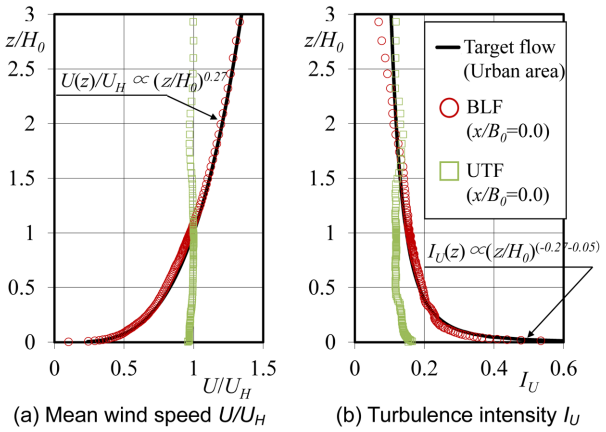
3.1. Speed-up Ratio and Speed-up Area

The pedestrian-level wind speed-up ratio R is given by Eq. (1) and the horizontal distribution of R is shown in Figs. 4 and 5.

$$R = \frac{Vel.mag.}{U_{z=2m}} \tag{1}$$

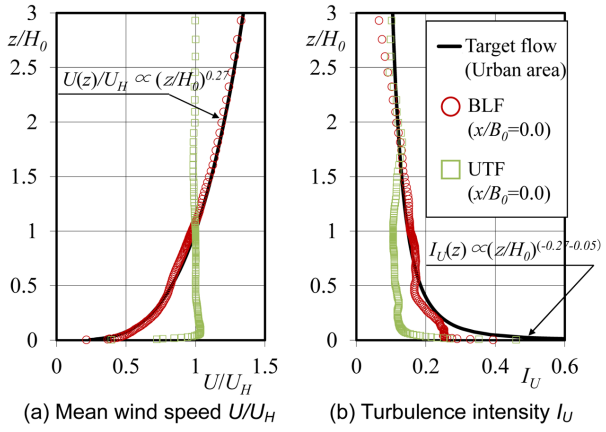
where *Vel.mag.* is the mean scalar wind speed defined as:

$$Vel.mag. = <vel.mag.> \tag{2}$$



(a) Mean wind speed U/U_H (b) Turbulence intensity I_U

Figure 2. Approaching flow conditions at inflow boundary, $x/B_0 = -30$

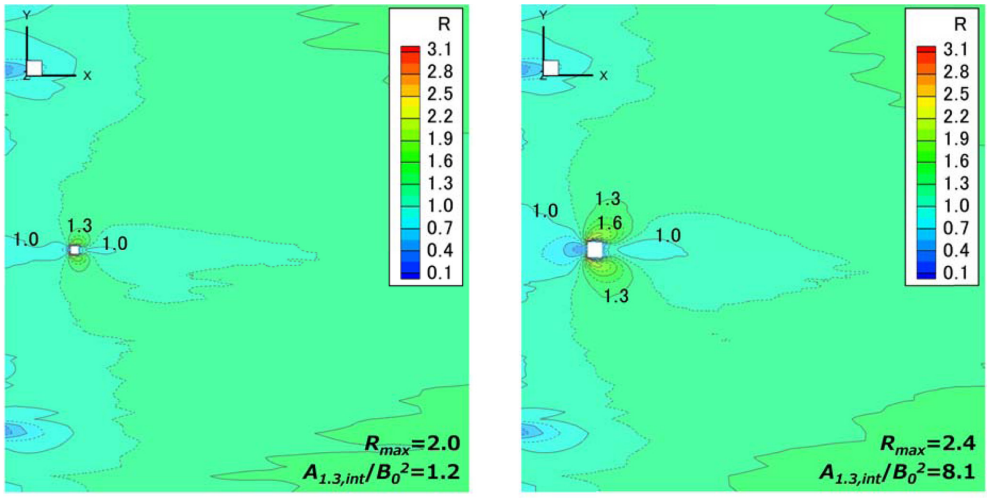


(a) Mean wind speed U/U_H (b) Turbulence intensity I_U

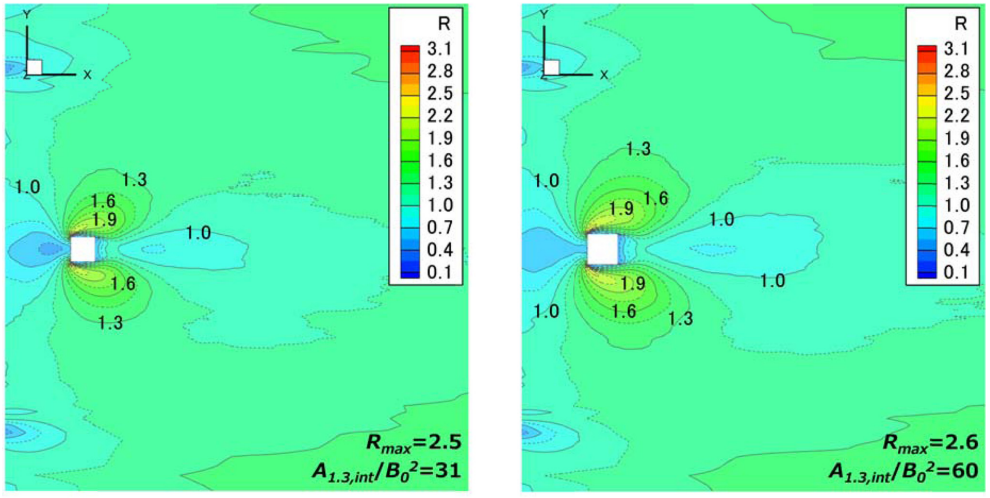
Figure 3. Approaching flow conditions at $x/B_0 = 0.0$

$$vel.mag. = \sqrt{u^2+v^2+w^2} \tag{3}$$

Here, *vel.mag.* is an instantaneous value of scalar wind speed and <*vel.mag.*> means the time average of *vel.mag.* The three components of momentary wind speed vector are defined as u (streamwise direction), v (across-wind direction) and w (vertical direction). Also, the time-

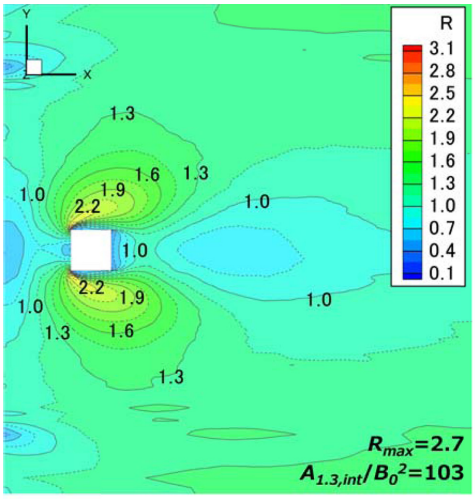


(a) B/H_0=0.0625(H_0/B=16) (b) B/H_0=0.125 (H_0/B=8)

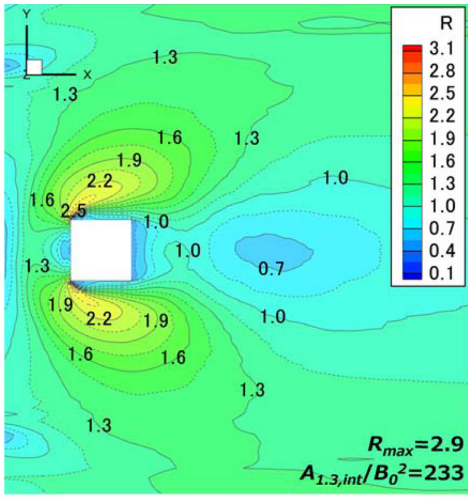


(c) B/H_0=0.2 (H_0/B=5) (d) B/H_0=0.25 (H_0/B=4)

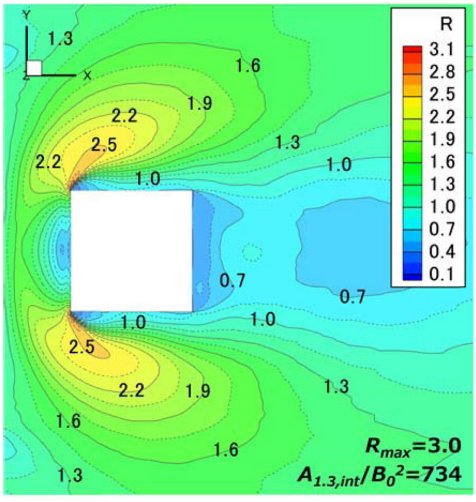
Figure 4. Distribution of speed-up ratio R at pedestrian-level for comparing difference of building width B (BLF).



(e) B/H_0=0.33 (H_0/B=3)



(f) B/H_0=0.5 (H_0/B=2)



(g) B/H_0=1 (H_0/B=1)

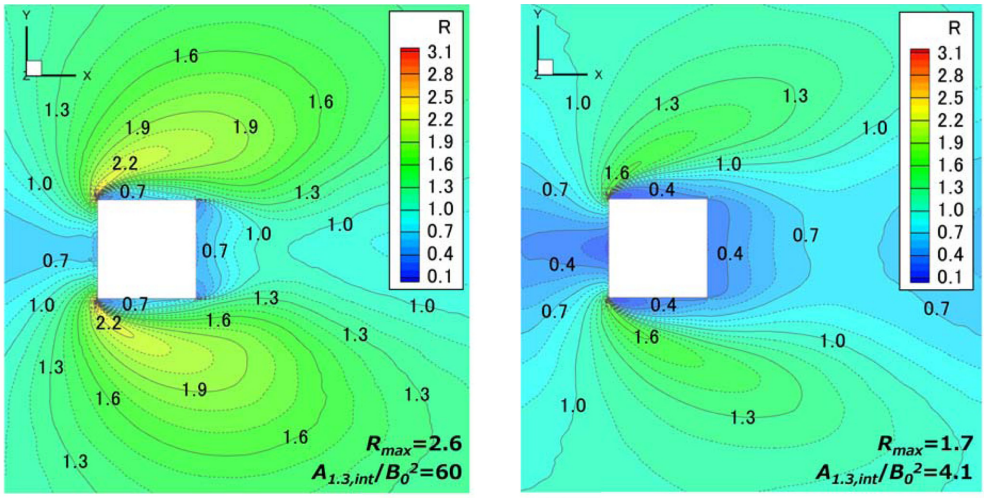
Figure 4. Distribution of speed-up ratio R at pedestrian-level for comparing difference of building width B (BLF). Continued.

averaged values of u, v, w are defined as U, V, W. $U_{z=2\,\mathrm{m}}$ is the mean wind speed in the streamwise direction at pedestrian level $z = 2$ m ($z/H_0 = 0.0125$).

As building height H_0 is constant, building width B alone affects the pedestrian-level wind speed. As shown in Figs. 4(a)~4(g), speed-up ratio R increases as width ratio B/H_0 increases, and the speed-up area also expands (for example, in the region where $R \geq 1.9$). This occurs because, under the same boundary layer flow (BLF), the three-dimensionality of flow patterns around buildings become more significant as building width B increases. The speed-up ratio R and the speed-up area around the building with $B/H_0 = 0.25$ in BLF are quite large compared with those around the same building in UTF, as shown in Figs. 5(a) and (b).

To demonstrate the above phenomena quantitatively, the variations of maximum speed-up ratio R_{max} and normalized speed-up area for $R \geq 1.3$, denoted as R_{max} and $A_{1.3,int}/B_0^2$, respectively, with width ratio B/H_0 are shown in Figs. 6 and 7, where $A_{1.3,int}$ represents the total area enclosed by the contour line for $R = 1.3$ on both sides of a building, and B_0^2 is the cross-sectional area of the building model with width ratio $B/H_0 = 0.125$ ($H_0/B = 8$). Figs. 6 and 7 also show the relationship between R_{max} and H_0/B, $A_{1.3,int.}/B_0^2$ and H_0/B, derived for buildings with $B/H_0 = 0.067$ to 0.25 ($H_0/B = 15$ to 4) from the wind tunnel test results of Tamura et al (2019).

The maximum speed-up ratio R_{max} increases with increase in width ratio B/H_0, as shown in Fig. 6, although the increasing rate gradually decreases and R_{max} saturates to around 3. As shown in Fig. 7, the normalized speed-up area $A_{1.3,int.}/B_0^2$ also increases with width ratio B/H_0, and the value of $A_{1.3,int.}/B_0^2$ becomes very large for larger B/H_0. Note that the ordinate for $A_{1.3,int.}/B_0^2$ is given in logarithmic scale. As an explanation of the variations of R_{max} and $A_{1.3,int.}/B_0^2$ with aspect ratio H_0/B shown in Figs.



(a) BLF (b) UTF

Figure 5. Distribution of speed-up ratio R at pedestrian-level for comparing BLF and UTF. ($B/H_0 = 0.25$ ($H_0/B = 4$))

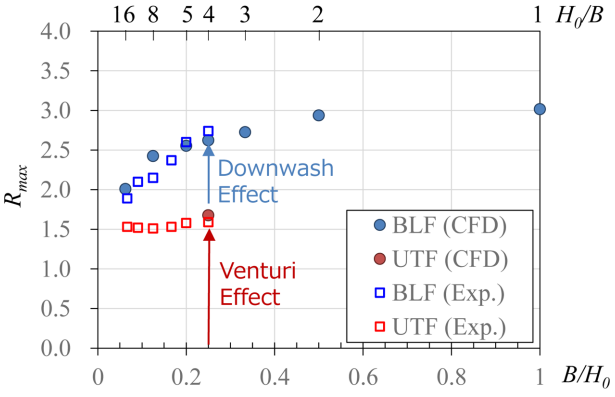


Figure 6. Relationship between width ratio B/H_0 and maximum wind speed-up ratio R_{max}. (The experimental results in the figure are referred with Tamura et al., 2019)

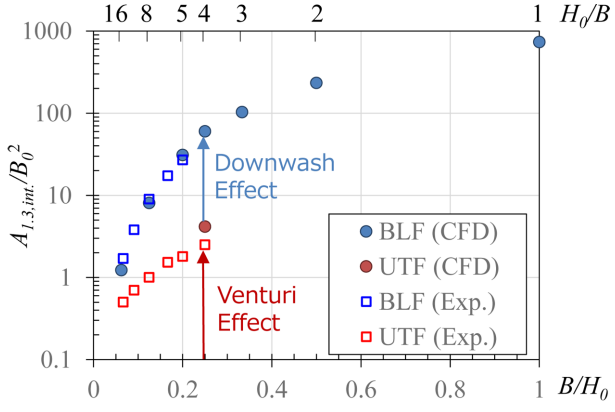


Figure 7. Relationship between width ratio B/H_0 and wind speed-up area $A_{1.3,int}/B_0^2$. (The experimental results in the figure are referred with Tamura et al., 2019)

6 and 7, Tamura et al. (2019) mentioned that the speed-up phenomenon was mainly caused by Venturi effect, and the variation of R_{max} with H_0/B for the building in UTF is not significant. Tamura et al. (2019) also mentioned that the difference between the speed-up ratios R for the buildings in BLF and UTF may be due to downwash effect. When building height H_0 is constant, the smaller the width ratio B/H_0, the stronger the two-dimensionality of the flow pattern around buildings, so R_{max} and $A_{1.3,\ int.}/B_0^2$ become smaller. Conversely, the downwash effect increases as the width ratio B/H_0 increases, because the flow pattern shows stronger three dimensionality. Therefore, it may be considered that the increasing downwash effect with increase in B/H_0 is the main reason for the larger values of R_{max} and $A_{1.3,int.}/B_0^2$ for buildings in BLF than those for buildings in UTF.

In response to this inference, this paper focuses on the flow pattern around the buildings using CFD simulation results, which are discussed below. The CFD results shown in Figs. 6 and 7 are comparable to the experimental results presented in Tamura et al. (2019), and this indicates that CFD results well reproduce the wind tunnel experimental results of Tamura et al. (2019). These results show that the discussion of the speed-up ratio and speed-up area based on CFD in this paper is appropriate.

3.2. Formation of Downflow and Three-dimensional Flow Field

Fig. 8 shows the distribution of non-dimensional vertical wind speed $W/U_{z=2m}$ at the vertical plane located at $0.05B$ from the windward surface of a building model ($x/B = -0.05$), where the mean vertical velocity component W is normalized by $U_{z=2m}$. The color contour indicates the intensity of the non-dimensional vertical wind speed $W/U_{z=2m}$. As shown in Fig. 8, upward flow occurs in the area where $W/U_{z=2m} > 0$ (green), and downward flow occurs in the area where $W/U_{z=2m} < 0$ (pink). When the width ratio B/H_0 is small, as shown in Figs. 8(a) and 8(b), $W/U_{z=2m}$ is close to zero over a wide range in the vertical direction, indicating a two-dimensional flow field with a

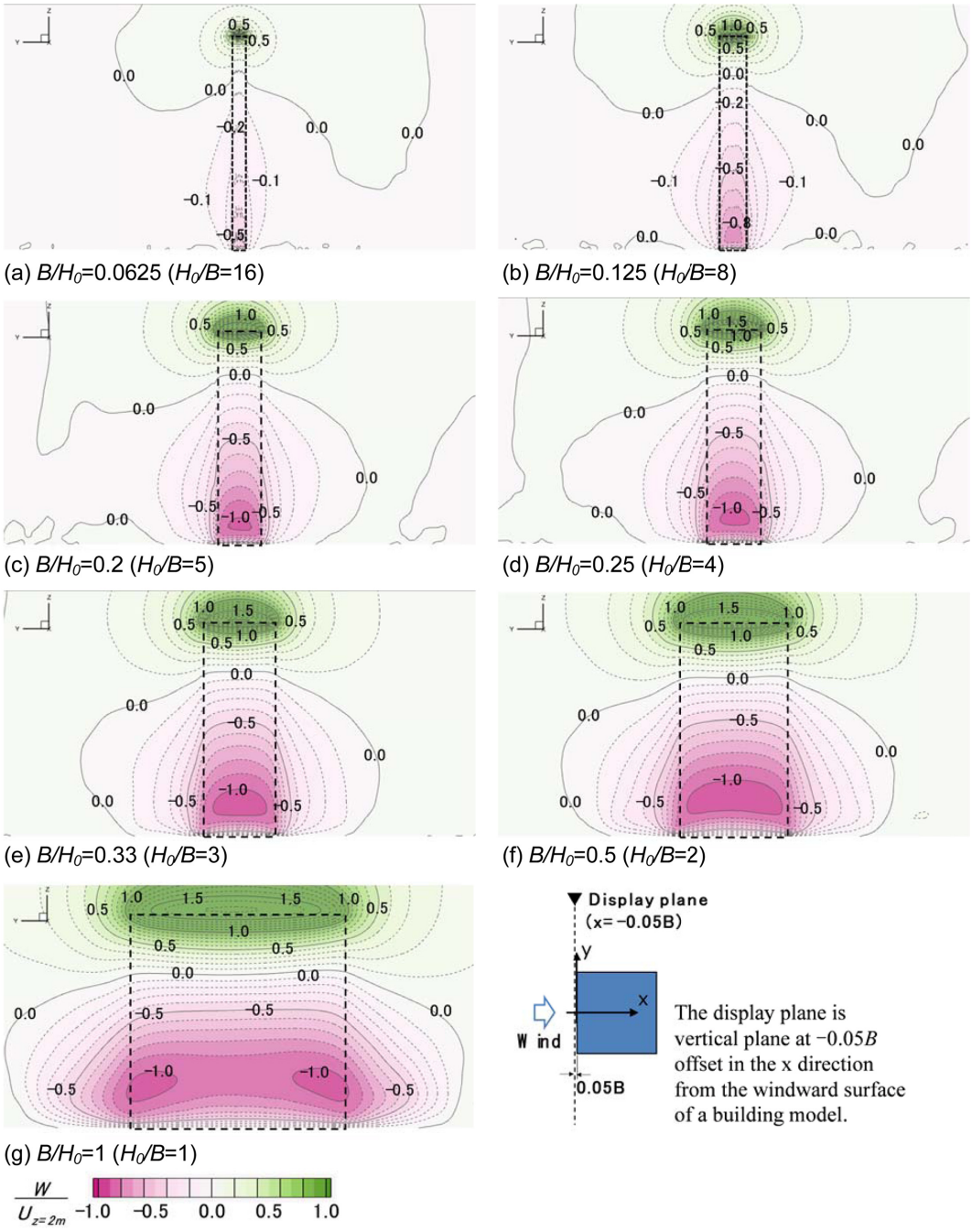


Figure 8. Distribution of nondimensional vertical wind speed $W/U_{z=2m}$ at vertical plane located at 0.05B from windward surface of a building model (x = –0.05B) for comparing difference of building width B (BLF)

small vertical wind speed. In addition, as B/H_0 increases, the area with a negative value of $W/U_{z=2m}$ gradually becomes darker in color and the downward wind speed increases, strengthening the flow's three-dimensionality. Especially in the case with $B/H_0 = 1$ shown in Fig. 8(g), areas with large downward velocity ($W/U_{z=2m} \leq -1.0$) appear on both sides of the lower parts of the building, which is different from other cases with width ratio $B/H_0 \leq 0.5$. The downward flow in the lower part of a building is blocked by the ground and basically flows outwards to both sides of the building. Thus, the downward flow becomes strong at the windward center of the building for the building with a small width ratio B/H_0. However, for a building with a large width ratio B/H_0 such as $B/H_0 = 1$, the downflow at the windward center blocked by the ground cannot easily go outward to the sides of the building, and the downflow speed is decreased near the ground by the blocking effect, as shown in Fig. 8(g). In contrast, the upward flows near the tops of the buildings can easily go over the roof regardless of width ratio B/H_0. Therefore,

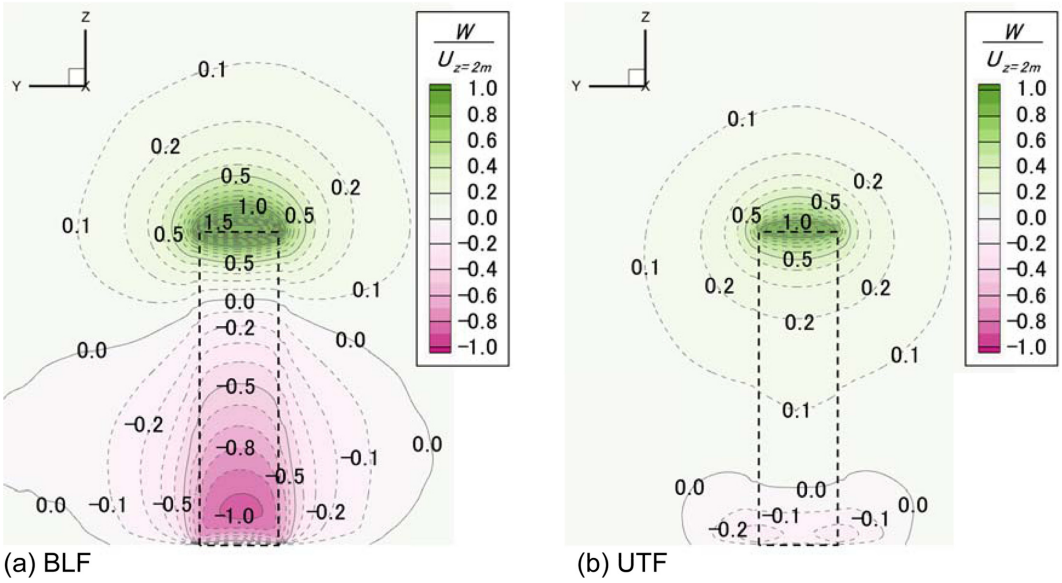


Figure 9. Distribution of nondimensional vertical wind speed $W/U_{z=2m}$ at vertical plane located at 0.05B from windward surface of a building model (x=–0.05B) for comparing BLF and UTF. ($B/H_0 = 0.25$ ($H_0/B = 4$))

there is no significant difference in the distribution of $W/U_{z=2m}$ at the top of the building for all building models with different B/H_0.

Next, Figs. 9(a) and (b) compare the distributions of $W/U_{z=2m}$ at the selected vertical plane for the reference building model (RBM) with $B/H_0 = 0.25$ ($H_0/B = 4$) in BLF and UTF. For the RBM in UTF, the values of $W/U_{z=2m}$ are close to 0 over a wide range almost centered at the height of the front stagnation point ($z/H_0 = 0.2$) and only downward flow occurs at around $z/H_0 = 0.1$, as shown in Fig. 9(b). In contrast, for the RBM in BLF, downward flow occurs over a wide range below the height of the front stagnation point around height $z/H_0 = 0.8$, as shown in Fig. 9(a). Therefore, it is reasonable to regard the flow field around the RBM in UTF as two-dimensional and the speed-up phenomenon in UTF is mainly due to the Venturi effect, as experimentally pointed out by Tamura et al. (2019). In contrast, the flow field around the RBM in BLF is more three-dimensional, and the contribution of downwash effect to the speed-up phenomenon is added to the Venturi effect in BLF. Similarly, downward flow below height $z/H_0 = 0.8$ can be observed for the building models in BLF with other aspect ratios. Thus, the difference between the maximum speed-up ratios for UTF and BLF shown in Fig. 6 and that of the normalized speed-up areas shown in Fig. 7 can be attributed to downwash effect.

Figs. 10 and 11 show the distribution of mean wind speed vectors $\overline{\boldsymbol{V}}(V,W)$ in the vertical plane located at 0.05B from the windward surface of a building model (x/B = –0.05). For all buildings in BLF, as mentioned earlier, downflows starting from the height $z/H_0 = 0.8$ due to the pressure gradient are observed, and strong side and downward flows are observed around the building corners (Figs. 10(a)-(g)). It is interesting that the flow at the central part near the base of the building with a large width ratio $B/H_0 = 1$ is restricted to the vertical direction because of the symmetric flow pattern, as shown in Fig. 10(g). Thus, the flow cannot easily go to the side of the building, and the downward flow is blocked by the ground, so the vertical flow speed cannot be high near the center of the building base. This is also clearly demonstrated in Fig. 10(g). Also compare the distributions of mean velocity vectors in the vertical plane for the RBM in BLF and UTF, as shown in Fig. 11(a) and Fig. 11(b), respectively. A three-dimensional downward flow field toward the sides is formed as shown in Fig. 11(a), while for the RBM in UTF shown in Fig. 11(b), an almost two-dimensional flow field is formed. The downward flow, as shown in Fig.11(a), is the downwash effect, which causes the acceleration phenomenon on both sides of the building. In the two-dimensional horizontal flow shown in Fig. 11(b), it is considered that the acceleration phenomenon is caused by the convergence effect in the horizontal plane of the flow blocked by the building, that is, Venturi effect.

3.3. Downwash Effect on Pedestrian-level Wind Speeds

Figs. 12 and 13 show the vertical distributions of dimensionless wind speeds $W/U_{z=2m}$ and $Vel.mag./U_{z=2m}$ at position (x/B = –0.05, y/B = –0.5) near the building corner for buildings in BLF. In all cases, $W/U_{z=2m}$ shows negative values below $z/H_0 \leq 0.8$, indicating downward flows due to the pressure gradient. In addition, the larger the width ratio B/H_0, the stronger the downward flow. For the buildings with small width ratios $B/H_0 = 0.0625$ and 0.125, the downward flow component is small, and a more two-dimensional flow is suggested. In the vertical distributions of the scaler wind speeds $Vel.mag./U_{z=2m}$ shown in Fig. 13, wind speed profiles similar to the approaching flow

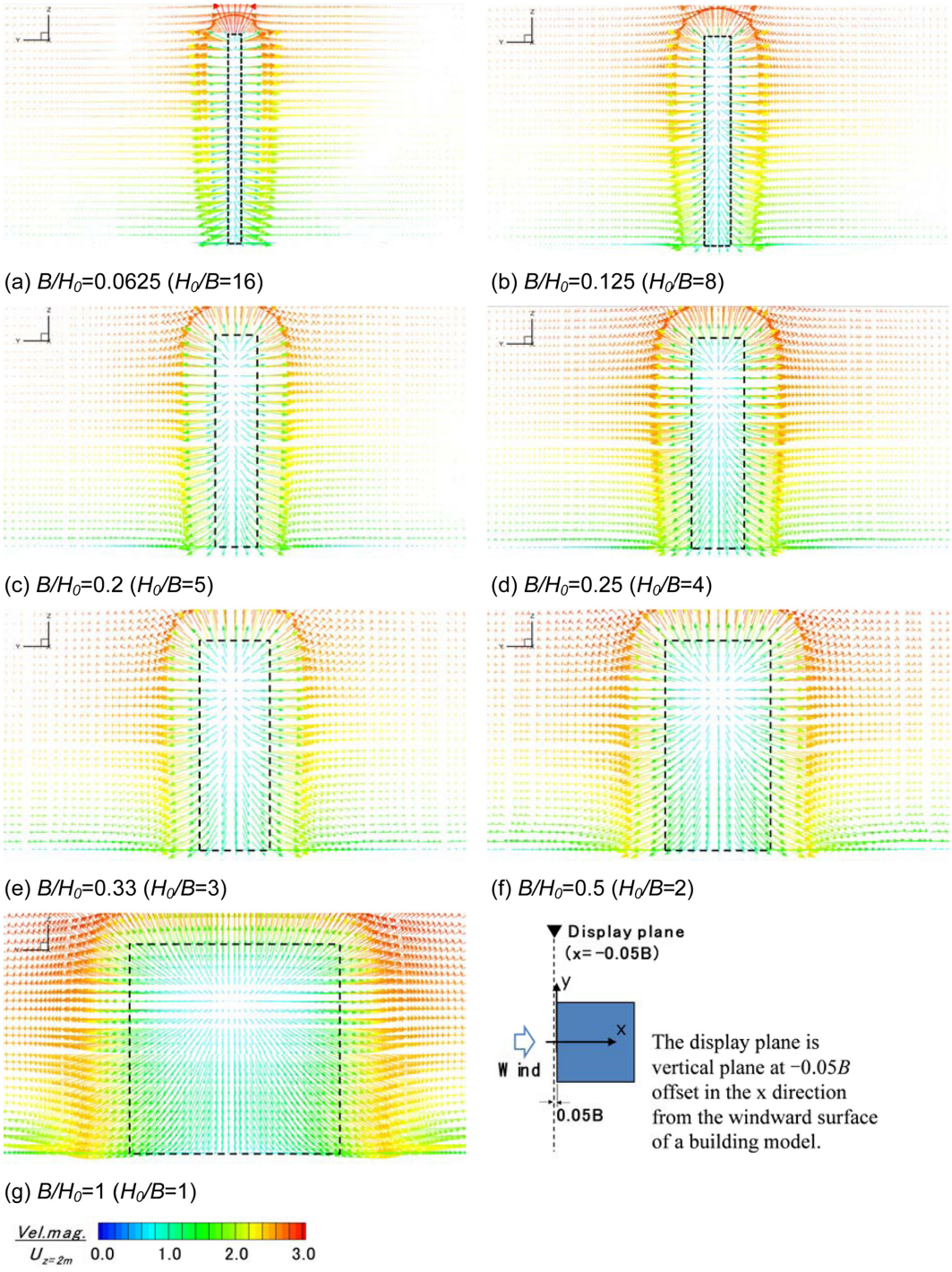


Figure 10. Distribution of mean wind speed vectors $\overline{\boldsymbol{V}}(V,W)$ in vertical plane located at 0.05B from windward surface of a building model ($x/B = -0.05$) for comparing difference of building width B (BLF).

(see Fig. 3) are maintained for the small width ratios $B/H_0 = 0.0625$ and 0.125, and the pedestrian-level wind speeds $Vel.mag./U_{z=2m}$ (= R) are not so large. However, for buildings with larger width ratios $B/H_0 = 0.20$ to 0.33, the wind speeds near the ground become larger than those on the upper parts. This can be attributed to the strong side and downward flows near the corners of the building bases shown in Figs. 8 and 10 observed for the buildings with larger width ratios B/H_0. Tamura et al. (2019) assumed that the high wind speed near the front stagnation point goes down to ground level and stimulates the speed-up phenomena at the pedestrian level in BLF for buildings with large width ratio B/H_0. The mean scaler wind speed $Vel.mag./U_{z=2m}$ profiles that are almost uniform or slightly

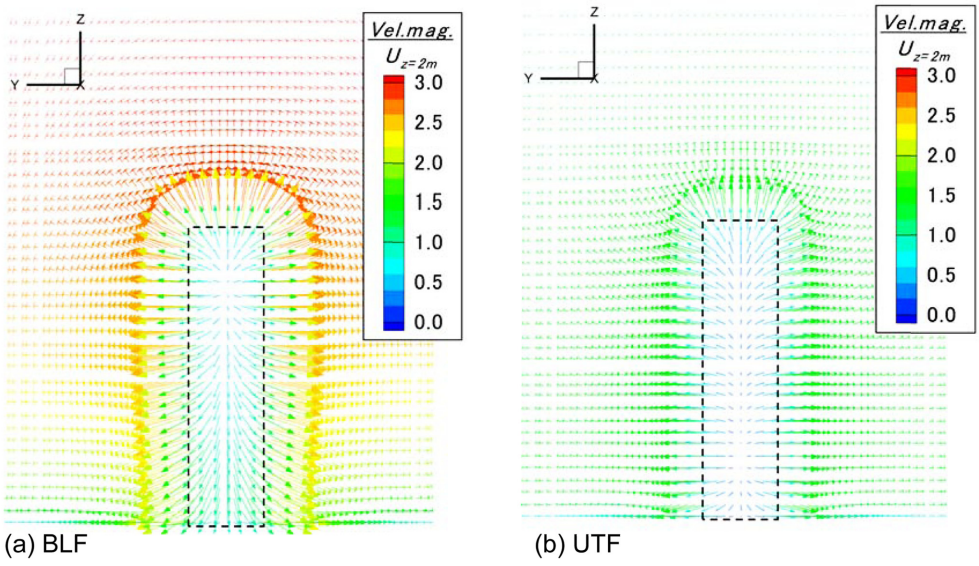


Figure 11. Distribution of mean wind speed vectors $\overline{V}(V,W)$ in vertical plane located at $0.05B$ from windward surface of a building model ($x/B = -0.05$) for comparing BLF and UTF ($B/H_0 = 0.25$ ($H_0/B = 4$))

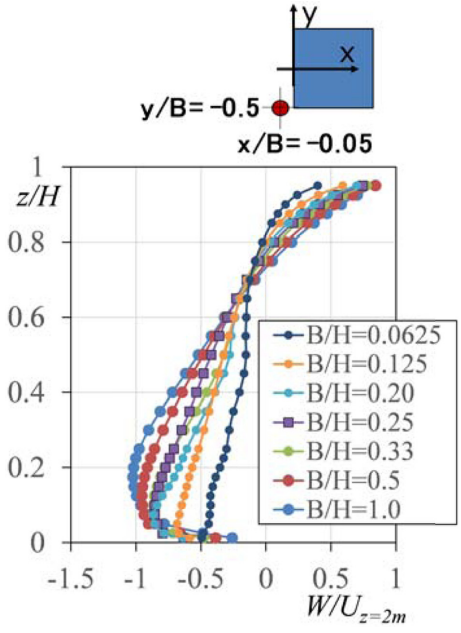


Figure 12. Vertical profile of mean vertical wind speed $W/U_{z=2m}$ near upwind corner of building.

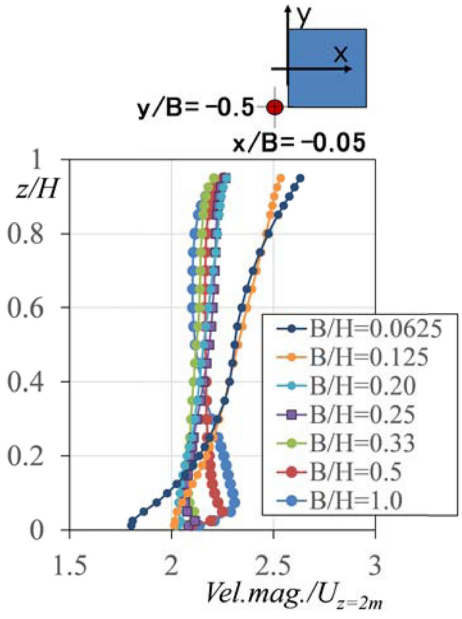


Figure 13. Vertical profile of mean scalar wind speed $Vel.mag./U_{z=2m}$ near upwind corner of building

larger at the lower level shown in Fig. 13 for buildings with large width ratios $B/H_0 = 0.2$-1.0 strongly support the assumption by Tamura et al. (2019). It is also confirmed that the variations of pedestrian-level mean wind speed distributions shown in Figs. 4 and 5 as well as the maximum speed-up ratio and the normalized speed-up area shown in Fig. 6 and Fig. 7, respectively, with building width ratio B/H_0 can be mainly attributed to the flow pattern change from 2D to 3D. Here, all the buildings have the same height H_0 and different widths B.

Fig. 14 shows the instantaneous streamlines around the building with width ratio $B/H_0 = 0.33$ (aspect ratio $H_0/B = 3$) and the instantaneous velocity vectors at the pedestrian-level. In Figs. 14(a)-(c), changes of wind flow are shown in a time series at non-dimensional time intervals $\Delta t U_{z=2m}/B = 0.35$. The color chart indicates the magnitude of the scaler wind speed $Vel.mag./U_{z=2m}$. It can be seen that the approaching flow turns into a downward flow at the windward surface of the building, and goes around the upwind corners at a high wind speed. When the downflow

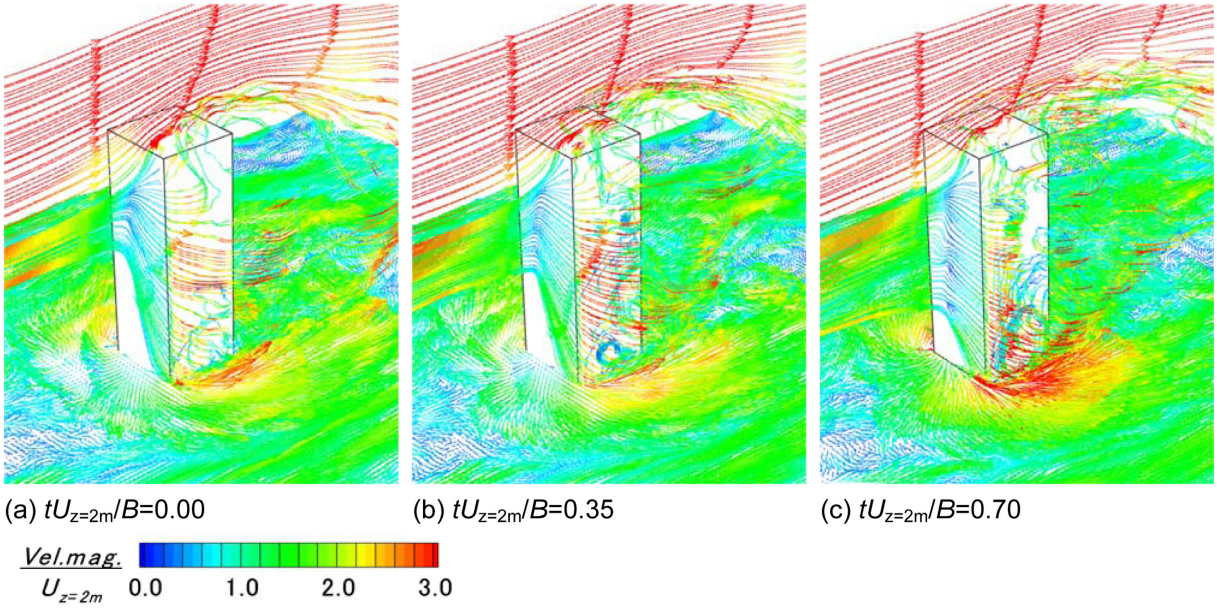


Figure 14. Distribution of instantaneous streamlines and pedestrian-level wind speed vectors $\overline{V}(u, v, w)$ around building with $B/H_0 = 0.33(H_0/B = 3)$

at the windward surface becomes large, a high wind speed appears at the pedestrian level near the building side. Furthermore, the strong sideward flow from the upwind corners formed in the upper layer gradually goes down. This flow reaches near ground level, and combines with the downflow at the windward surface, forming a wide higher wind speed area at pedestrian level near the building side.

4. Concluding Remarks

Tamura et al. (2019) experimentally studied pedestrian-level mean wind speeds and found that there are two types of variations of downwash effects: the 2D – 3D flow pattern change (Type 1) according to the building aspect ratio H_0/B (or width ratio B/H_0); and the captured wind speed change near the front stagnation point (Type 2) due to the size effects of buildings with the same aspect ratio (or width ratio). In this study, CFD simulations using LES were conducted to verify the Type 1 variation of downwash effect reported by Tamura et al. (2019) by observing the flow patterns around building models with different width ratios B/H_0. The contributions of downwash effect and Venturi effect were also examined based on flow pattern observations. The following results were obtained based on a series of CFD results in which the building models had constant height $H_0 = 160$ m and different widths B, giving width ratios $B/H_0 = 0.0625$~1.

CFD results of the maximum speed-up ratio R_{max} and normalized speed-up area $A_{1.3,int.}/B_0^2$ of pedestrian-level winds agree well with those of experimentally obtained wind tunnel results by Tamura et al. (2019), which indicates high reproducibility of LES to corresponding wind tunnel experiment results. Thus, the reliability of the present study of flow patterns based on CFD results was verified.

Downward components of wind velocities in the vertical plane located at $0.05B$ from the windward surface of the RBM in UTF are limited to very close to ground level, and the majority of the building portion shows almost 2D flow pattern. Thus, the speed-up phenomenon in UTF is mainly caused by the Venturi effect due to the flow conversion in the horizontal plane. However, for the RBM in BLF, downward flows occur in the major part below $z/H_0 = 0.8$. The speed-up phenomenon in BLF is significantly contributed to by the downwash effect, in addition to the Venturi effect.

For buildings with small width ratios $B/H_0 = 0.0625$, 0.125 ($H_0/B = 16$, 8), downward flows are small and tend to show 2D flow patterns, mean wind speed profiles similar to the approaching wind are maintained, and pedestrian-level winds are not much enhanced by downwash effect.

For buildings with relatively large width ratios $B/H_0 = 0.2$ to 1.0 ($H_0/B = 5$ to 1), the mean wind speed near the ground is similar to that in the upper levels or intensified due to downwash effect, and pedestrian-level winds become higher.

Thus, we can conclude that the discussions on the two types of variations of downwash effects experimentally made by Tamura et al. (2019) are basically supported by this flow pattern study based on CFD, at least for the Type 1 variation.

Acknowledgements

This research is part of the research of a research group with Professor Akihito Yoshida of Tokyo Polytechnic

University, and we hereby express our gratitude to him. Part of this research used the computational resources of the supercomputer Fugaku provided by the RIKEN Center for Computational Science (Project ID: hp210292). Part of this research was funded by the scholarship from China Scholarship Council (No. 202006050113).

References

Architectural Institute of Japan, (2016). AIJ Benchmarks for Validation of CFD Simulations Applied to Pedestrian Wind Environment around Buildings.

Beranek, W. J., (1984). Wind environment around single buildings of rectangular shape, Heron, 29(1): 1-31.

Blocken, B., (2014). 50 years of computational wind engineering: past, present and future. Journal of Wind Engineering and Industrial Aerodynamics, 129, 69-102.

Blocken, B., (2018). LES over RANS in building simulation for outdoor and indoor applications: A foregone conclusion? Building Simulation, 11, 821-870.

Blocken, B., Moonen, P., Stathopoulos, T., Carmeliet, J., (2008). Numerical study on the existence of the venturi effect in passages between perpendicular buildings. Journal of Engineering Mechanics, 134(12), 1021-1028.

Bourgeois, J. A., Sattari, P., Martinuzzi, R. J., (2011). Alternating half-loop shedding in the turbulent wake of a finite surface-mounted square cylinder with a thin boundary layer. Physics of Fluids, 23(9), 095101.

Cao, Y., Tamura, T., Large-eddy simulations of flow past a square cylinder using structured and unstructured grids, Computers and Fluids 137, 36-54.

Cook, N. J., (1985). The Designer's Guide to Wind Loading of Building Structures, Background, Damage Survey, Wind Data and Structural Classification. Building Research Establishment Report.

Cui, D., Hu, G., Ai, Z., Du, Y., Mak, C. M., Kwok, K. (2019). Particle image velocimetry measurement and CFD simulation of pedestrian level wind environment around U-type street canyon. Building and Environment, 154(5), 239-251.

Du, Y., Mak, C. M., Kwok, K., Tse, K. T., Lee, T. C., Ai, Z., et al. (2017). New criteria for assessing low wind environment at pedestrian level in Hong Kong. Building & Environment, 123: 23-36.

Hooff, T. V., Blocken, B., Tominaga, T., On the accuracy of CFD simulations of cross-ventilation flows for a generic isolated building: comparison of RANS, LES and experiments, Building and Environment, 114, 148-165.

Hu, G., Tse, K. T., Kwok, K., Zhang, Y. (2015). Large eddy simulation of flow around an inclined finite square cylinder. Journal of Wind Engineering and Industrial Aerodynamics, 146: 172-184.

Isyumov, N., Davenport, A.G., (1975). Comparison of Full-scale and Wind Tunnel Wind Speed Measurements in the Commerce Court Plaza, Journal of Wind Engineering and Industrial Aerodynamics, 1, 201-212.

Isyumov, N., Davenport, A.G., (1975). The ground level wind environment in built-up areas, in: Proceedings of Fourth International Conference on Wind Effects on Buildings and Structures, London, pp. 403-422

Kajishima, T. (1999). Finite-Difference Method for Convective Terms using Non-Uniform Grid. Transactions of the JSME (in Japanese), Vol.65(633), p103-108.

Kamei, I., Maruta, E., (1979). Study on wind environmental problems caused around buildings in Japan. Journal of Wind Engineering and Industrial Aerodynamics, 4(3), 307-331.

Kawai, H., Okuda, Y., Ohashi, M., (2012). Near wake structure behind a 3d square prism with the aspect ratio of 2.7 in a shallow boundary layer flow. Journal of Wind Engineering and Industrial Aerodynamics, 104-106, 196-202.

Kim, B., Tse, K. T., Yoshida, A., Chen, Z., Phuc, P. V., Park, H. S., (2019). Investigation of flow visualization around linked tall buildings with circular sections. Building and Environment, 153(3), 60-76.

Kobayashi, H. (2005). The subgrid-scale models based on coherent structures for turbulent channel flow, Phys. Fluids 17, 045104.

T.V. Lawson, The wind content of the built environment, Journal of Wind Engineering and Industrial Aerodynamics, 3, 93-105.

Lawson, T.V., Penwarden, A.D., (1975). "The Effects of Wind on People in the Vicinity of Buildings." Proc. the 4th International Conference on Wind Effects on Buildings and Structures, Cambridge University Press, Heathrow, pp. 605-622.

Liu, J., Niu, J., CFD simulation of the wind environment around an isolated high-rise building: an evaluation of SRANS, LES and DES models, Building and Environment 96, 91–106.

Liu, Z., Yu, Z., Chen, X., Cao, R., Zhu, F. (2020). An investigation on external airflow around low-rise building with various roof types: PIV measurements and LES simulations. Building and Environment, 169(2), 106583.1-106583.20.

Maruyama, T. (2004). Numerical Calculation of Turbulent Boundary Layer over Rough Surface using Large Eddy Simulation, Proceedings of the 18th National Symposium on Wind Engineering, p57-62.

Melbourne, W.H. (1978). Criteria for environmental wind conditions, Journal of Wind Engineering and Industrial Aerodynamics, 3, 241-249.

Murakami, S., Iwasa, Y., Morikawa, Y., (1986). Study on acceptable criteria for assessing wind environment at ground level based on residents' diaries. Journal of Wind Engineering and Industrial Aerodynamics, 24(1), 1-18.

Murakami, S., Uehara, K., Komine, H., (1979). Amplification of wind speed at ground level due to construction of high-rise building in urban area. Journal of Wind Engineering and Industrial Aerodynamics, 4(3), 343-370.

NEN, (2006). Wind Comfort and Wind Danger in the Built Environment, NEN 8100 (In Dutch) Dutch Standard.

Sumner, D., Rostamy, N., Bergstrom, D. J., Bugg, J. D., (2017). Influence of aspect ratio on the mean flow field of a surface-mounted finite-height square prism. International Journal of Heat and Fluid Flow, 65, 1-20.

Tamura, Y., Xu, X., Yang, Q., (2019). Characteristics of pedestrian-level mean wind speed around square buildings:

effects of height, width, size and approaching flow profile. Journal of Wind Engineering and Industrial Aerodynamics, 192, 74-87.

Tanaka, H., Tamura, Y., Ohtake, K. Nakai ,M., Kim,Y.C. and Bandi, E.K. (2013). Aerodynamic and Flow Characteristics of Tall Buildings with Various Unconventional Configurations. International Journal of High-Rise Buildings, Vol.2, No.3, p213-228.

Tanaka, H., Konno, N., Ohtake, K. and Tsuchiya, N. (2014). Prediction Accuracy of Wind Forces Acting on High-rise Buildings in Urban Areas by Large Eddy Simulation, Proceedings of the 6th International Symposium on Computational Wind Engineering in Hamburg.

Tominaga, Y., Blocken, B., (2015). Wind tunnel experiments on cross-ventilation flow of a generic building with contaminant dispersion in unsheltered and sheltered conditions, Build and Environment, 92, 452-461.

Tominaga, Y., Mochida, A., Yoshie, R., Kataoka, H., Nozu, T., Yoshikawa, M., et al., (2008). AIJ guidelines for practical applications of CFD to pedestrian wind environment around buildings. Journal of Wind Engineering and Industrial Aerodynamics, 96(10-11), 1749-1761.

Tsang, C.W., Kwok, K.C.S., Hitchcock, P.A., 2012. Wind tunnel study of pedestrian level wind environment around tall buildings: effects of building dimensions, separation and podium. Building and Environment, 49, 167-181.

Wang, H. F., Zhou, Y., Chan, C. K., Lam, K. S., (2006). Effect of initial conditions on interaction between a boundary layer and a wall-mounted finite-length-cylinder wake. Physics of Fluids, 18(6), 065106.

Wise, A.F.E., (1970). "Wind Effects Due to Groups of Buildings.", Proc. the Royal Society Symposium Architectural Aerodynamics, Session 3, Effect of Buildings on the Local wind, London, February, pp. 26-27.

Xu, X., Yang, Q., Yoshida, A., Tamura, Y., (2017). Characteristics of pedestrian-level wind around super-tall buildings with various configurations. Journal of Wind Engineering and Industrial Aerodynamics, 166, 61-73.

Yoshie, R., Mochida, A., Tominaga, Y., Kataoka, H., Harimoto, K., Nozu, T., et al., (2007). Cooperative project for CFD prediction of pedestrian wind environment in the Architectural Institute of Japan. Journal of Wind Engineering and Industrial Aerodynamics, 95(9-11), 1551-1578.